Integration of CFD Tools in Aerodynamic Design of Contra-Rotating Propeller Blades

S. Béchet and C. A. Negulescu
Airbus Operations S.A.S. - Aerodynamics Department, Toulouse, France

V. Chapin
ISAE DAEP, Toulouse, France

F. Simon
ONERA DMAE, Toulouse, France

Keywords: *Contra-Rotating Propellers, Open Rotors, Blades, Aerodynamic Design, CFD*

Abstract

A strategy for Contra-Rotating Open Rotors blades design is presented. It is based on several analytical or Computational Fluid Dynamics (CFD) tools with increasing levels of accuracy. A preliminary design is made with a lifting-line code. These first geometries are then validated and improved with more advanced CFD methods. Steady CFD computations on a blade passage using the mixing-plane technique permit to perform an accurate sensitivity analysis of the main blade geometrical parameters. The key parameters driving the propulsive efficiency are thus identified.

Modeling rotor-rotor interactions require more costly unsteady simulations such as chorochronic computations on a blade passage, or chimera/sliding-mesh techniques on the full model to assess the installation effects. At the end of the design process, these unsteady methods are used to validate the robustness of the advanced designs to those interactions.

The relevance of this strategy is discussed through its results and limitations.

Nomenclature

ρ	air density [kg/m^3]
γ	air adiabatic coefficient
a	celerity of sound [m/s]
N	front propeller rotational speed [rev/s]
ω	angular speed [rad/s]
D	front propeller diameter [m]
r	radial location [m]
R	propeller tip radius [m]
J	front propeller advance ratio
V	infinite inflow velocity [m/s]
p	static pressure [Pa]
M_∞	infinite Mach number
Cth	thrust coefficient
Cp	power coefficient
η	propulsive efficiency
$._F$	variable related to front rotor
$._R$	variable related to aft/rear rotor
$._{SEC}$	variable related to blade section

1 Introduction

Contra-Rotating Open Rotors (CROR) are highly efficient aircraft propulsion systems [1]. This concept promises significant reductions of fuel consumption and pollutant emissions. Its interest is highlighted by the current context of economic and environmental concerns. After a

period of fruitful developments and tests performed in the US during the '80s in response to the oil crisis of that period, interest in CROR decreased and they finally never reached the commercial aviation.

Current economic and environmental objectives have led aeronautical industry to put new research efforts into that concept which is a candidate for next generation short-range aircraft propulsion systems. Emphasis is put on the development of experimental and numerical methods dedicated to better understand and predict CROR aero-acoustic behavior.

The CROR propeller design is a complex task as it involves multidisciplinary aspects like aerodynamic, acoustic and structural concerns. Already for an isolated engine the strong front/rear rotors aerodynamic wake and potential field interactions cause unsteady flow on the blades and interaction noise. These interactions are even more significant in installed conditions on the aircraft. Indeed, depending on the chosen configuration and because of the presence of the pylon, wing, and due to aircraft incidence, the propeller inflow is not uniform. Therefore the flow on the blades presents even more unsteadiness and will impact not only the aerodynamic performances, but also the acoustic emissions and the structural integrity of the propeller.

This paper presents the development of a CFD-based strategy for aerodynamic design of CROR blades. Nowadays several types of numerical methods and levels of modeling are available. Fast techniques such as lifting line methods have been widely used up to now [2]. However these methods are not sufficient any more, even though they remain valid for preliminary design. A higher level of accuracy is sought and can be found in more advanced CFD methods able to simulate the complete three-dimensional viscous flow and even its unsteadiness.

Two kinds of CFD methods need to be considered. Firstly, because the design process requires many iterations there is a strong need for a flexible mesh generation and short-time response CFD. Secondly, a deeper analysis is performed with costly unsteady computations in order to validate a specific configuration.

The following paragraphs present these different methods and show how they are used to conduct a complete design process. Besides, results are presented that can be expected at each step.

2 Preliminary Design

The first step of CROR blades design aims to define a preliminary set of reference geometries respecting global aerodynamic performance, installation, structural and acoustic constraints.

2.1 Operating conditions

Two conditions are considered in the design process:

- Cruise: Mach 0.75 / RPM 795 / Alt 35kft
- Take-off: Mach 0.20 / RPM 1032 / Alt 0ft

2.2 Performances

The different designs have to fulfil the cruise and take-off propeller thrust requirements. That sets the global thrust coefficient:

$$Cth = \frac{Thrust_{GLOBAL}}{\rho . N^2 . D^4} \qquad (1)$$

Engine considerations also fix the power ratio between the front (F) and rear (R) rotors:

$$\frac{Cp_F}{Cp_R} = \frac{Power_F}{Power_R} = \frac{Torque_F . \omega_F}{Torque_R . \omega_R} \qquad (2)$$

These requirements will be satisfied during the iterative design process by adapting the front and rear propeller pitch angles β_F and β_R.

The aerodynamic performance of each design is given by the propeller propulsive efficiency:

$$\eta = J . \frac{Cth}{Cp} = \frac{V}{N.D} \frac{Cth}{Cp} \qquad (3)$$

The objective of the design process is to optimize this efficiency.

2.3 Reference propeller dimensions

For a 150-seat single aisle short range aircraft with a rear-mounted pusher engine configuration, installation concerns limit the diameter of the propellers to 14 feet. A high value is preferable both for performances and acoustics. For acoustic reasons, the rear rotor diameter is lowered by 10% in order to reduce its interaction with the front rotor tip vortex. To maintain the aft propeller blade surface its blade chord is increased.

Front and rear rotor blade numbers, which are the results of a compromise between aerodynamics and acoustics, have been chosen as 11 and 9 respectively. For the same reasons, the distance between front and rear rotors planes is set to 950 mm.

2.4 Definition of the blade shape

The shape of the blade is defined by the following radial blade laws distributions:

- Airfoil type
- Chord (m)
- Relative camber (% of chord)
- Relative thickness (% of chord)
- Twist angle (°)
- Sweep angle (°)
- Dihedral (m)

Structural considerations associated to reference geometries found in literature permit to define a relative thickness (decreasing from a minimum foot value to a minimum tip value) and chord distribution. At the same time, an airfoil type is selected as a compromise between the different operating conditions of the propeller (e.g supercritical airfoil).

The first lifting line computations with the code LPC2 from ONERA [3] are now performed at high and low speed conditions with imposed target thrust and power ratio with a convergence on pitch angle settings. Some iterations are necessary to determine camber and twist distributions that give at high speed the target load distribution (e.g. Goldstein load distribution [4]). Fig. 1 shows the limitations of the modeling of the load distribution (especially a root and tip) using this lifting line code.

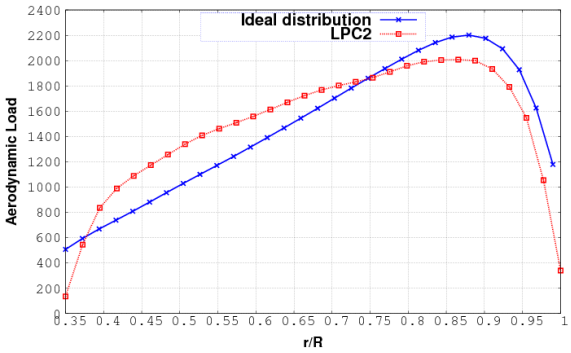

Fig. 1 Aerodynamic load distribution computed with lifting line method compared to ideal distribution

The final step is made through a new series of lifting line computations to find a more adequate sweep distribution in order to reduce the compressibility losses and increase the efficiency. For structural considerations, one has to be careful that the blades remain balanced around their pitch change axis.

Even though the quality of the lifting line solution is questionable, this first step is important because the design choices made at the beginning may condition the further results obtained with more accurate methods.

2.5 Reference configuration

This approach has led to the AI-PX7 11x9 CROR blades design. The blades are mounted on a representative nacelle dummy (Fig. 2). This configuration will be used as reference for further steps of the design. This is also a current reference configuration for the European SFWA/CleanSky project[1].

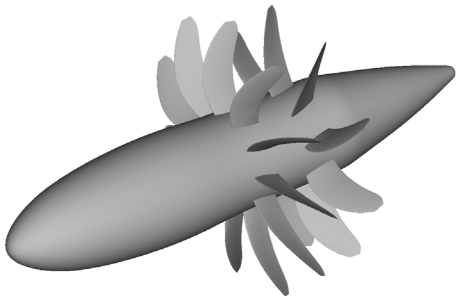

Fig. 2 AI-PX7 CROR Configuration

[1] http://www.cleansky.eu/

The upstream infinite Mach number was adjusted in order to have M=0.75 in the propeller plane (i.e. aircraft installed conditions).

3 Detailed design

In a second phase the goal is to enhance the aerodynamic performances of the proposed CROR. This is done through an analysis based on more accurate CFD tools which are able to simulate the 3D steady flow on the blades.

3.1 Mixing plane technique

The first approach consists in performing steady RANS computations on a limited-size grid using the mixing plane technique in the ONERA code *elsA* [5].

Each rotor is restricted to one inter-blade passage. The flow is solved in the rotating frame. At the interface between front and aft rotor grids, data is azimuthally averaged along a mixing plane. On the lateral boundaries periodic boundary conditions are set.

In contrast to a full unsteady modeling the steady-state mixing plane approach does not permit to simulate the interactions between the propellers, as well as any incidence or installation effects. Only steady load is known and this restricts any future acoustic evaluation to steady load and shock noise assessment.

However, such a method is well adapted for an aerodynamic design purpose, as it gives access to the 3D blade flow within a short computation time.

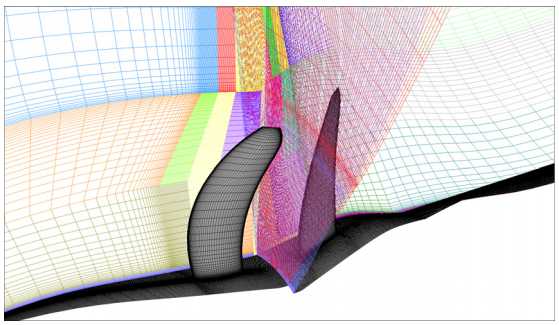

Fig. 3 Structured mesh on AI-PX7 configuration (mixing plane technique)

3.2 Automatic process

The interest of this kind of intermediate method is its ability to compute a high number of configurations. This can be even more efficient if the CFD solver is embedded inside an automatic process also including CAD and mesh generation tools. This design strategy is adopted here.

This automatic process is very important, as the extension of this work will be the integration of the parametrical design process into an aerodynamic and finally an aero-acoustic optimization process.

3.2.1 Blade parameterization

The first step of such an automatic process is to generate the blade shape. All the parameters previously defined in Section 2.4, as well as the pitch angles of the front and aft blades, are controlled. The goal is to respect with the highest possible accuracy the target radial blade laws distributions by an adequate set of control sections (Fig. 4).

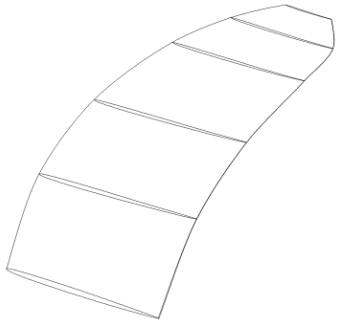

Fig. 4 AI-PX7 Front Blade Parameterization

The in-house tool *PADGE* (Parametrical And Differentiated Geometrical Engine) [6] uses these control sections to reconstruct the complete blade surface. The generation of the shape is ensured by the use of *NURBS* (Non-Uniform Rational Basis Splines) calculated between sections with tangency constraints at the sections location. One strong interest of this method is the capacity to control and modify the shape with the relevant parameters defining the blade shape.

3.2.2 Initial mesh

The geometry obtained through this parameterization tool is mounted on the nacelle and the structured multi-block mesh is generated, with a boundary layer mesh both on blades and nacelle. It has been shown that a 4 million nodes grid for the front and rear inter-blade passage is sufficient to perform an aerodynamic study of the CROR.

3.2.3 Mesh deformation

This reference mesh is an input for the initialization of the blade shape parameterization tool. From this point on, any modification of a parameter (shape or pitch angle) is treated through the in-house tool *VOLDEF* (VOLume mesh DEFormation) [7] as a displacement of the surface nodes and propagated in the volume mesh until the boundary of the domain. The displacement of the boundaries can be limited or even forbidden. This is particularly important for periodic sub-faces and the mixing plane.

3.2.4 RANS computations

Computations are run on the *elsA* CFD solver from ONERA. The study is performed with the Sparlart-Allmaras one-equation turbulence model.

3.2.5 Post-processed data

Propeller performances analysis requires essentially post-processing of pressure and friction data on the surface of the blades. Integration gives access to the aerodynamic forces and moments and so to the front, aft and global performances coefficients *Cth*, *Cp* and η.

For local analysis of the flow on the blades, the pressure coefficient taking into account the relative velocity due to the propeller rotation is defined as:

$$Kp_{ROT} = 2\frac{(p_\infty - p)}{\gamma . p_\infty . M_{rel}^2} \qquad (4)$$

with :

$$M_{rel}^2 = M_\infty^2 + M_{rot}^2 = M_\infty^2 + \frac{r^2 . \omega^2}{a_\infty^2} \qquad (5)$$

The radial distributions of lift and drag coefficients are defined as:

$$Cl(r) = 2\frac{Fl_{SEC}}{\gamma . p_\infty . M_{rel}^2(r) . c(r)} \qquad (6)$$

$$Cd(r) = 2\frac{Fd_{SEC}}{\gamma . p_\infty . M_{rel}^2(r) . c(r)} \qquad (7)$$

with Fl_{SEC} and Fd_{SEC} the radial section forces (taking into account the pressure and friction contributions) respectively normal and tangent to the profile chord whose length is *c*.

3.3 Pitch angles adaptation

As previously stated, the blades have to provide the required thrust and power ratio. As the RPM is fixed, the only way to respect those specifications is to find the adapted pitch angle settings on both rotors. These settings cannot be known directly. For each rotor a minimal and a maximal pitch angles must be defined such as the corresponding thrust and power ratio ranges will always include the target values for different blade shapes. As explained in Fig. 5, four computations are needed and adapted pitch angles are found by a linear interpolation.

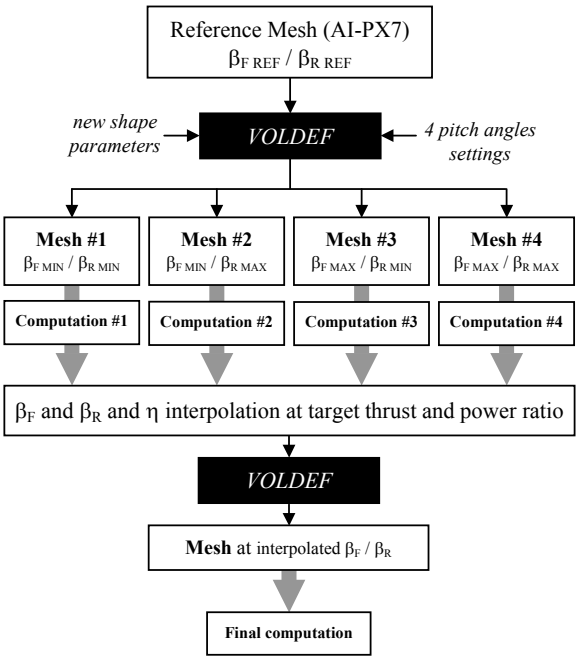

Fig. 5 Aerodynamic Computations Process

For simplicity reasons, the same extreme pitch angle values are taken for front and aft rotors. These have been estimated by the lifting line method with ±5% variations on the target thrust and power ratio.

A final computation is then done with the interpolated pitch angles giving thus access to the blades aerodynamic at the required operating conditions.

3.4 Sensitivity analysis

In the following paragraphs some results of a sensitivity analysis are presented. Shape modifications are performed on the AI-PX7 reference configuration. The objective is to identify some geometrical modifications that influence significantly the aerodynamic propeller performances (efficiency) at high speed.

The choice of each modification is either a consequence of the analysis of the reference configuration, for which weaknesses and potential improvements have been identified, or it is due to an external constraint such as structural or acoustic.

It has to be mentioned here that the level of impact of some of the parameters depends strongly on the reference design layout.

3.4.1 Effect of chord modification

A first interesting test is to scale the front and aft chord distributions by a global factor. Table 1 highlights the potential efficiency increase that can be obtained with a smaller surface, confirming the fact that the blades are not working at the optimal L/D ratio.

Table 1 Efficiency evolution for chord modification

Case	Efficiency (vs. reference)	β_{FRONT}	β_{AFT}
+10% on global chord	-0.40%	-0.19°	-0.11°
+5% on global chord	-0.19%	-0.10°	-0.05°
-5% on global chord	+0.18%	+0.11°	+0.06°
-10% on global chord	+0.34%	+0.23°	+0.12°

3.4.2 Effect of sweep modification

Sweep angle is now increased at the tip of front and aft blades to reduce the local Mach number and thus the shocks intensity. As it appears on Table 2, no significant effect is noticed on the propeller efficiency for an 8° or a 14° tip sweep increase.

Table 2 Efficiency evolution for tip sweep modification

Case	Efficiency (vs. reference)	β_{FRONT}	β_{AFT}
+8° on tip sweep	-0.04%	-0.03°	+0.03°
+14° on tip sweep	-0.04%	-0.01°	+0.08°

In a second step, the sweep distribution is increased all over the blade except at the tip. This is done keeping 0° sweep at r/R=55% and increasing the negative blade root sweep by -4°. Table 3 reports an insignificant effect. Apparently, increasing the sweep (locally or globally) has no major effect on the efficiency. The reference blade has obviously already a sufficient sweep level and therefore no strong shocks (Fig. 6).

Table 3 Efficiency evolution for sweep modification

Case	Efficiency (vs. reference)	β_{FRONT}	β_{AFT}
Scaled sweep	+0.02%	+0.05°	+0.03°

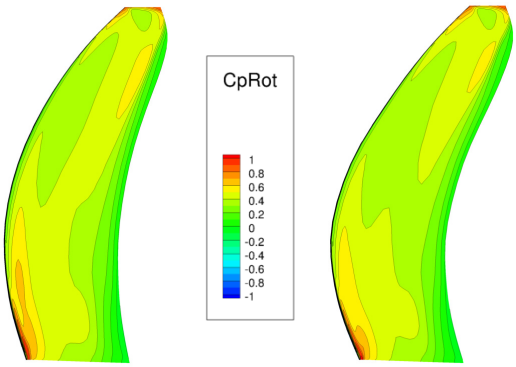

Fig. 6 Front blade suction side pressure coefficient distribution (reference vs. scaled sweep)

3.4.3 Effect of twist modification

A direct way to modify the load distribution is to change the root and tip blade twist. Two

tests are performed here: first the tip twist is decreased by 3.2°, secondly the root twist is diminished by 2.3°. Both cases correspond to a local load reduction. A third case combines these two modifications.

Effects on efficiency are presented in Table 4. It appears that a lower twist angle at blade tip increases the efficiency. On the other side the blade root twist modification decreases the efficiency. This can be explained by a better matching or respectively by a deviation from the optimal blade loading distribution. The combination of these two modifications has consequently no effect on the efficiency.

Table 4 Efficiency evolution for twist modification

Case	Efficiency (vs. reference)	β_{FRONT}	β_{AFT}
-3.2° on tip twist	+0.28%	+0.05°	+0.11°
-2.3° on root twist	-0.41%	+0.12°	+0.17°
-3.2° on tip twist and -2.3° on root twist	-0.10%	+0.17°	+0.28°

3.4.4 Effect of camber modification

Front blade camber level has been defined during the preliminary design step to fulfil take-off thrust requirements. The margin was significant, so the camber is likely to be diminished. A -30% factor is applied on the front camber distribution to assess the potential benefits.

As presented in Table 5, the loss of lift is recuperated by a large front pitch angle increase. Decreasing the blade camber level results in a profile drag reduction and so an increase of efficiency (Fig. 7).

Table 5 Efficiency evolution for camber modification

Case	Efficiency (vs. reference)	β_{FRONT}	β_{AFT}
-30% on front camber	+0.42%	+0.64°	-0.05°

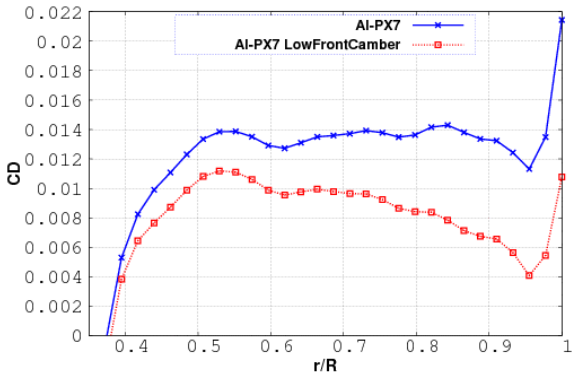

Fig. 7 Front blade sectional drag coefficient radial distribution (reference vs. lower camber)

3.4.5 Effect of thickness modification

Manufacturing or structural constraints are likely to limit the blade thickness to a minimal value. Two tests are therefore performed to assess the impact of such a modification. In the first case the blades are regularly thickened along the whole span to reach 1% more relative thickness at blade tip compared to the reference geometry. In the second case the blades are thickened starting from r/R=80% to the tip where there is a 0.5% increase of relative thickness.

Table 6 shows the deterioration of the performances in the first case, mainly caused by a drag increase.

Table 6 Efficiency evolution for thickness modification

Case	Efficiency (vs. reference)	β_{FRONT}	β_{AFT}
Global thickness increase (up to +1% relative thickness)	-0.47%	+0.04°	-0.01°
+0.5% tip relative thickness	-0.06%	< 0.01°	< 0.01°

In the second case the impact is very low. Actually, the reference blade tip is already very thin, and this result demonstrates that there is a margin to increase tip thickness without impacting the efficiency.

4 Unsteady computations

As a last step of the aerodynamic design process the robustness of the blade design to

flow non-homogeneities due to front/rear rotor interactions and installation effects (here incidence effect) has to be assessed.

The objective is to check that the performances of blades previously designed with the RANS iterative design process are still satisfactory under these unsteady flow conditions. This analysis is here performed by unsteady computations on the full model of the AI-PX7 configuration using the elsA solver.

4.1 Chimera technique

One suitable way is to perform URANS computations with the Chimera mesh technique [8]. Here, a background grid plus two cylindrical rotating grids for each rotor are linked through overlap regions as depicted in Fig. 8. Variables exchange between the different grids is done by interpolations in the overlap regions.

The interest of this technique is the ability to use a well-adapted grid with an adequate refinement on the blades without impacting the density in the background mesh. Moreover new geometries can be quite easily assessed replacing only the Chimera grids.

First applications of this technique on CROR have been published by Stuermer and al. [9][10][11]. The work performed on the Airbus AI-PX7 propeller is an application of recent developments and studies made by François and al. [12] who have defined best practices for such computations with the elsA solver.

4.2 Computations

The elsA solver is used to perform unsteady simulations on a 53 million nodes mesh with boundary layer meshing. For the performances assessment, the choice has been made to use a time step equivalent to 2 degrees of rotation, in order to simulate the main fluctuations associated to rotor-rotor interactions and incidence effect.

Starting from a converged solution (obtained after three rotations), an additional rotation is computed to get a converged cycle.

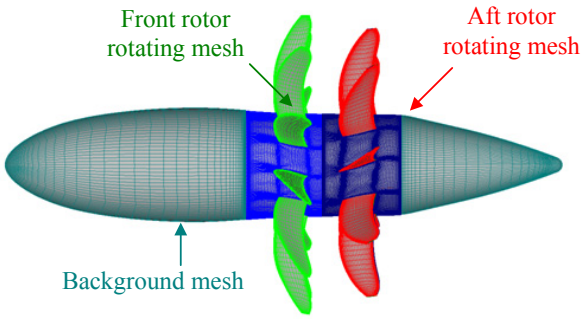

Fig. 8 Chimera mesh on AI-PX7 Configuration

4.3 Propulsion performances

As for the RANS computations, the first check is made on the performances. Such simulations provide reliable results on forces fluctuations encountered by a blade, at least for the first harmonics of the incidence effects and rotor/rotor interactions [12]. However Fig. 9 highlights, on the example of the thrust coefficient, the balancing that appears when taking into account the complete propellers. Only negligible rotor-rotor interaction fluctuations can still be observed. The result is the same for fluctuations linked to incidence effect, for which a slight increase of mean thrust appears (only 0.3% with a 2° angle of attack).

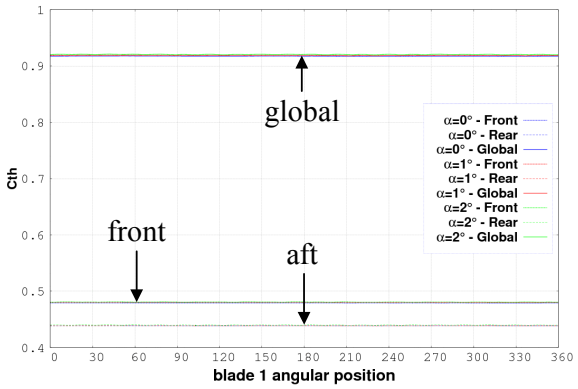

Fig. 9 Front, aft and global thrust coefficient fluctuations for 0°, 1° and 2° incidences

4.4 Aerodynamic field on blades

In addition to global performances it is interesting to observe the local unsteady aerodynamic phenomena occurring on blades. This can help in identifying parts of the blades that are not robust and are source of too much

deterioration of performances in unsteady conditions.

The analysis of the pressure field gives a good description of the flow. Fluctuations related to incidence effect can be observed on Fig. 10. Front blade 75% radial section pressure coefficient cuts are plotted for incidences 0, 1 and 2 degrees for the angular positions 120° and 290° which approximately correspond to the minimal and maximal load positions. For zero-incidence there is only a slight fluctuation, which is caused by the potential field interactions with the aft rotor. For 1° and 2° incidences, the rotor-rotor interaction fluctuations are weak compared to those related to the incidence effect whose period is one propeller rotation.

Those unsteady effects can also be observed on the aerodynamic load distributions (Fig. 11). In the present case, a good robustness of the blade can be noticed because there is no drop in the load distribution. Of course these fluctuations may have a significant impact on structural integrity or acoustic emissions and should be mastered but this is not the scope of this paper.

For the aft blade (Fig. 12 and Fig. 13), the same kind of fluctuations can be noticed. However, the amplitude related to the incidence effect (once per rotation) seems to be a bit less pronounced. This is due to the front rotor, which straightens the flow. Once again no unfavorable behavior is observed.

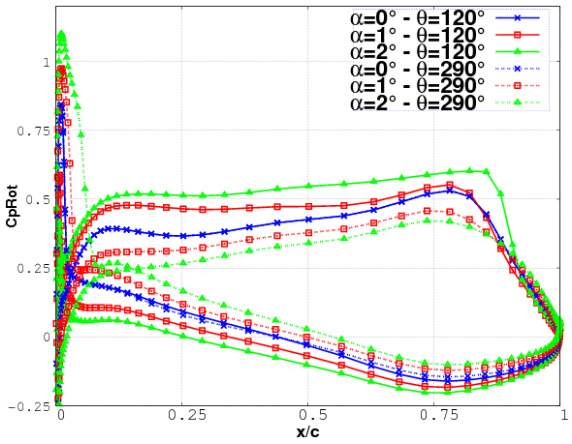

Fig. 10 Front blade pressure coefficient distribution (75% relative radial location) at 120° and 290° angular position (incidences 0, 1 and 2°)

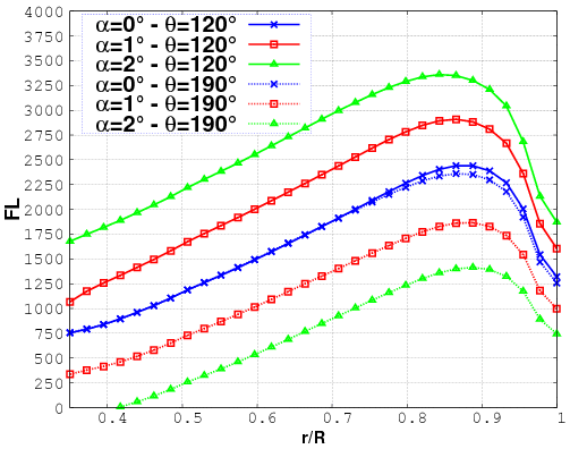

Fig. 11 Front blade radial aerodynamic load distributions at 120° and 290° angular position (incidences 0, 1 and 2°)

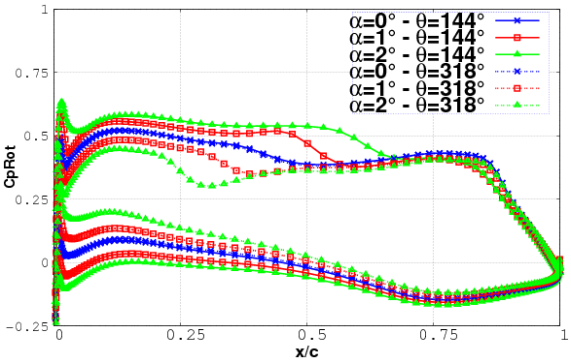

Fig. 12 Aft blade pressure coefficient cuts (75% relative radial location) at 144° and 318° angular position (incidences 0, 1 and 2°)

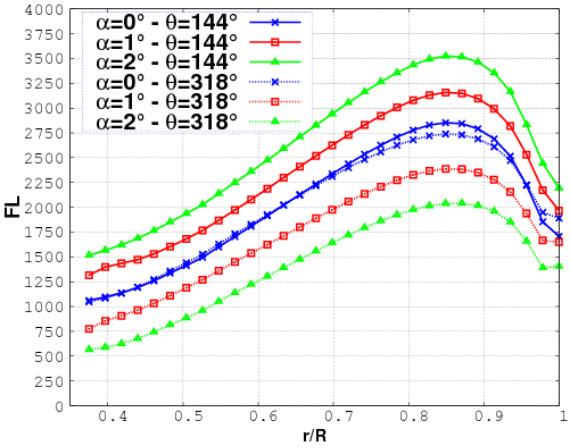

Fig. 13 Aft blade radial aerodynamic load distributions at 144° and 318° angular position (incidences 0, 1 and 2°)

A stronger impact of the incidence effect can be seen at the front blade root where the shock intensity is strongly increasing for 2° for the down-going blade (Fig. 14). Nevertheless no flow detachment is observed.

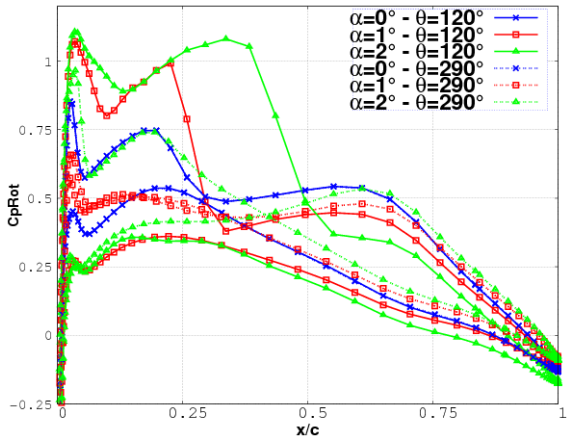

Fig. 14 Front blade pressure coefficient distribution (40% relative radial location) at 120° and 290° angular position (incidences 0, 1 and 2°)

5 Conclusion

A complete aerodynamic CROR blades design process has been presented. The lifting line approach permits to define a reference geometry. The performed RANS sensitivity study gives an idea about the main blade shape parameters influencing the propulsive efficiency. The unsteady computations analysis permits to focus on critical blades areas.

Extensions of this work will be the integration of the parametrical design process into an aerodynamic and finally an aero-acoustic optimization process as Marinus and Roger [13] or Pagano and al. [14] did on single-rotating propellers.

Acknowledgements

This work is carried out in the frame of a PhD thesis funded by Airbus. Authors would like to thank the Airbus Aerodynamics Methods and Tools Team for their work on CFD for CROR applications and tools dedicated to shape parameterization and mesh deformation.

References

[1] Hager R.D., Vrabel D., "Advanced turboprop project", *NASA Technical Report*, 1988.

[2] Saito S., Kobayashi H., and Nasu K., "Performance Calculation of Counter Rotation Propeller". Proceeding in 16th AIAA/CEAS Aeroacoustics Conference, 2010.

[3] Bousquet J. M., "Theoretical and experimental analysis of highspeed propeller aerodynamics". Proceeding in *AIAA/ASME/SAE/ASEE 22nd Joint Propulsion Conference*, 1986.

[4] Goldstein S., "On the Vortex Theory of Screw Propellers", *Proceedings of the Royal Society A,* 1929, pp. 440-465.

[5] Cambier L. and Gazaix M., "elsA: an efficient object-oriented solution to CFD complexity" Proceeding in *40th AIAA Aerospace Science Meeting and Exhibit*, 2002.

[6] PADGE User Manual.

[7] VOLDEF User Manual.

[8] Steger J., Dougherty F.C., Benek J.A., "A chimera grid scheme, Advances in grid generation". Proceeding of the *Applied Mechanics, Bioengineering and Fluids Engineering Conference*, 1983.

[9] Stuermer A., "Unsteady CFD Simulations of Contra-Rotating Propeller Propulsion Systems". Proceeding in *44th AIAA/ASME/SAE/ASEE Joint Propulsion Conference & Exhibit*, 2008.

[10] Stuermer A. and Yin J., "Low-Speed Aerodynamics and Aeroacoustics of CROR". Proceeding in *15th AIAA/CEAS Aeroacoustics Conference*, 2009.

[11] Stuermer A. and Yin J., "Aerodynamic and Aeroacoustic Installation Effects for Pusher-Configuration CROR Propulsion Systems". Proceeding in *28th AIAA Applied Aerodynamics Conference*, 2010.

[12] François B., Costes M. and Dufour G., "Comparison of Chimera and Sliding Mesh Techniques for Unsteady Simulations of Counter Rotating Open-Rotors". Proceeding in *20th ISABE Conference*, 2011.

[13] Marinus B.G. and Roger M., "Aeroacoustic and Aerodynamic Optimization of Aircraft Propeller Blades". Proceeding in *16th AIAA/CEAS Aeroacoustics Conference*, 2010.

[14] Pagano A., Federico L., Barbarino M., Guida F. and Aversano M., "Multi-objective Aeroacoustic Optimization of an Aircraft Propeller". Proceeding in *12th AIAA/ISSMO Multidisciplinary Analysis and Optimization Conference*, 2008.